

Multilevel Neural Network DTC with Balancing Strategy of Sensorless DSSM Using Extended Kalman Filter

Benyoussef Elakhdar^{1,✉}, Barkat Said², and Radhwane Sadouni³

¹Faculty of Science Applied, Department of Electrical Engineering, University of Kasdi Merbah, Ouargla

²(Faculty of Technology, Department of Electrical Engineering, University of M'sila

³Material, Energy Systems Technology and Environment Laboratory, University of Ghardaia, Algeria

✉ lakhdarbenyoussef@yahoo.com

Abstract

This paper presents direct torque control based on artificial neural networks of a double star synchronous machine without mechanical speed and stator flux linkage sensors. The estimation is performed using the extended Kalman filter, which is known for its ability to process noisy discrete measurements. The proposed approach consists of replacing the switching tables with one artificial neural network controller. The output vector of the artificial neural network controller is directed to a multilevel switching table to decide which reference vector should be applied to control the two five-level diode-clamped inverters. This inverter topology has the inherent problem of DC-link capacitor voltage variations. Multilevel direct torque control based on a neural network with balancing strategy is proposed to suppress the unbalance of DC-link capacitor voltages. The simulation results presented in this paper highlight the improvements offered by the proposed control method based on the extended Kalman filter under various operating conditions.

Keywords: Double Star Synchronous Machine, Multilevel Inverter, Direct Torque Control, Artificial Neural Networks Control, Extended Kalman Filter.

1 Introduction

Over the past decade, multiphase variable-speed drives have attracted increasing interest from researchers. Multiphase machines have major applications, such as electric ship propulsion, aircraft drives, locomotive traction and high power industrial plants, and require high power ratings for both the motor and its converter [1].

Among multiphase machines, the double star synchronous machine (DSSM) has two star-winding supplied by two independent voltage source inverters [2]. Two-level or multilevel inverters may be used.

There are several types of multilevel inverters. The diode-clamped, flying capacitor, and cascade H-bridge

are the prevailing multilevel topologies. In particular, the diode-clamped inverter (DCI) has been found to be suitable for adjustable speed drives [3]. However, this kind of multilevel DCI suffers from DC-link capacitor voltage unbalance [4]. Various remedial measures are reported in the technical literature [5], [6].

On the other hand, the direct torque control (DTC) method is known for its simple implementation and fast dynamic response [2]. The main advantages of DTC are the absence of coordinate transformation and the absence of a separate voltage modulator [7]. Common disadvantages of DTC using hysteresis controllers are the large current and torque ripples and high current distortion [8]. To overcome this problem, many contributions have focused on artificial intelligence based DTC [7], [9]. However, few papers have yet sought to extend the DTC based on an artificial neural network (DTC-ANN) to multilevel topologies [10].

Several speed observers have been suggested in the literature, such as sliding mode observer [11], adaptive observer, model reference adaptive system, and extended Kalman filter [12]. The Kalman filter is a stochastic state observer where nonlinear equations are linearized in every sampling period. It has the advantage of providing both flux and speed estimates, and thus avoids the limitations of the open loop pure integration method.

In order to balance DC-link capacitor voltages and to ensure high performance of the multiphase drive, the five-level DTC-ANN with balancing strategy is applied on sensorless DSSM using the extended Kalman filter (EKF).

This paper is organized as follows: the model of the DSSM is presented in section 2. In section 3, the five-level DCI model is described. In section 4, the five-level DTC strategy is illustrated. The EKF algorithm is introduced in brief in section 5. The switching tables used in conventional five-level DTC are sub-

stituted by an artificial neural networks controller in section 6. Section 7 is devoted to the simulation results for five-level DTC-ANN. Section 8 covers the balancing control strategy of DC-link capacitor voltages. The simulation results of sensorless five-level DTC-ANN with balancing strategy are discussed in section 9. Finally, conclusions are drawn in the last section.

2 Modeling of the DSSM

The DSSM model is based on the assumption that space harmonics and magnetic saturation are negligible, and that the two stator three-phase windings are identical and symmetrical, with the two neutrals being isolated. To derive a mathematical model suitable for control, the following transformation matrix is used, as proposed in [2].

$$[A] = \frac{1}{\sqrt{3}} \begin{bmatrix} 1 & -\frac{1}{2} & -\frac{1}{2} & \frac{\sqrt{3}}{2} & -\frac{\sqrt{3}}{2} & 0 \\ 0 & \frac{\sqrt{3}}{2} & -\frac{\sqrt{3}}{2} & \frac{1}{2} & \frac{1}{2} & -1 \\ 1 & -\frac{1}{2} & -\frac{1}{2} & -\frac{\sqrt{3}}{2} & \frac{\sqrt{3}}{2} & 0 \\ 0 & -\frac{\sqrt{3}}{2} & \frac{\sqrt{3}}{2} & \frac{1}{2} & \frac{1}{2} & -1 \\ 1 & 1 & 1 & 0 & 0 & 0 \\ 0 & 0 & 0 & 1 & 1 & 1 \end{bmatrix} \quad (1)$$

By using this transformation, the dynamic model describing the machine in reference can be given by:

$$\begin{cases} V_\alpha = R_s \cdot i_\alpha + L_q \frac{di_\alpha}{dt} - w \cdot \phi_f \cdot \sin(\theta) \\ V_\beta = R_s \cdot i_\beta + L_q \frac{di_\beta}{dt} + w \cdot \phi_f \cdot \cos(\theta) \end{cases} \quad (2)$$

With:

V_α, V_β : The α - β components of stator voltage.

i_α, i_β : The components of stator current.

ϕ_f : Flux of rotor excitation.

The rotor voltage equation is given by:

$$V_f = R_f \cdot i_f + \frac{d\phi_f}{dt} \quad (3)$$

Where V_f, i_f : DC voltage and DC current of rotor excitation.

The mechanical equation is expressed by:

$$J \cdot \frac{d\Omega}{dt} = T_{em} - T_L - f \cdot \Omega \quad (4)$$

With:

T_{em}, T_L : Electromagnetic and load torque.

Ω : Rotor speed.

The electromagnetic torque is given by:

$$T_{em} = p(\phi_\alpha \cdot i_\beta - \phi_\beta \cdot i_\alpha) \quad (5)$$

With:

ϕ_α, ϕ_β : The components of stator flux.

p : The pole-pair number.

3 Modeling of the Five-level DCI

Figure 1 shows the structure of a five-level DCI (only one leg is presented). The voltage across each capacitor is $v_{dc}/4$ and each device voltage stress will be limited to one capacitor voltage level through clamping diodes [4].

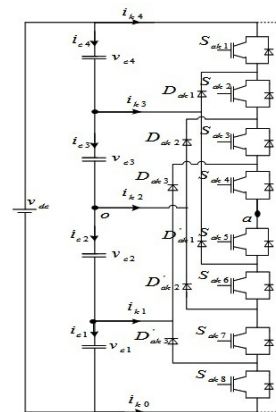


Figure 1: Circuit diagram of a phase leg for a five-level DCI ($k=1$ for first inverter and $k=2$ for second inverter)

Since five kinds of switching states exist in each phase, the five-level inverter has 125 switching states and there are 61 effective vectors, as shown in figure 2

Table 1: Switching state of five-level DCI (x=a, b or c)

State	Sxk1	Sxk2	Sxk3	Sxk4	Sxk5	Sxk6	Sxk7	Sxk8	Vxk0
4	1	1	1	1	0	0	0	0	Vc3+Vc4
3	0	1	1	1	1	0	0	0	Vc3
2	0	0	1	1	1	1	0	0	0
1	0	0	0	1	1	1	1	0	-Vc2
0	0	0	0	0	1	1	1	1	-(Vc1+Vc2)

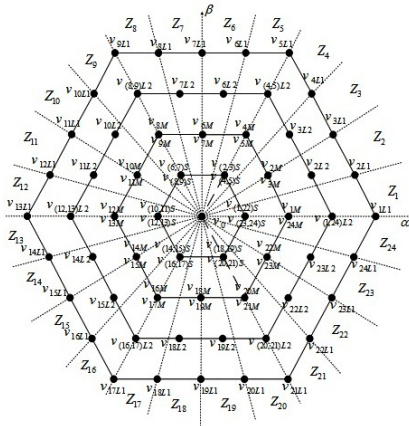


Figure 2: Space voltage vectors for a five-level diode DCI

The function switch is modeled by a Boolean function F_{xki} defined by:

$$F_{xki} = \begin{cases} 1 & S_{xkj} \text{ is ON} \\ 0 & S_{xkj} \text{ is OF} \end{cases} \quad j = 1 : 8 \quad (6)$$

For each leg of the inverter, five connections functions can be defined as follows:

$$\begin{cases} F_{cxk1} = F_{xk1} \cdot F_{xk2} \cdot F_{xk3} \cdot F_{xk4} \\ F_{cxk2} = F_{xk2} \cdot F_{xk3} \cdot F_{xk4} \cdot F_{xk5} \\ F_{cxk3} = F_{xk3} \cdot F_{xk4} \cdot F_{xk5} \cdot F_{xk6} \\ F_{cxk4} = F_{xk4} \cdot F_{xk5} \cdot F_{xk6} \cdot F_{xk7} \\ F_{cxk5} = F_{xk5} \cdot F_{xk6} \cdot F_{xk7} \cdot F_{xk8} \end{cases} \quad (7)$$

The phase voltages v_{ak} , v_{bk} , v_{ck} can be written as:

$$\begin{bmatrix} v_{ak} \\ v_{bk} \\ v_{ck} \end{bmatrix} = \begin{bmatrix} F_{cak1} & F_{cak2} & F_{cak3} & F_{cak4} & F_{cak5} \\ F_{cbk1} & F_{cbk2} & F_{cbk3} & F_{cbk4} & F_{cbk5} \\ F_{cck1} & F_{cck2} & F_{cck3} & F_{cck4} & F_{cck5} \end{bmatrix} \begin{bmatrix} v_{c3} + v_{c4} \\ v_{c3} \\ 0 \\ -v_{c2} \\ -(v_{c1} + v_{c2}) \end{bmatrix} \quad (8)$$

4 Direct Torque Control Strategy

The basic principle of DTC is to directly manipulate the flux vector so that the desired torque is produced, this control strategy permits to control directly and independently the ux and the electromagnetic torque. This is achieved by choosing a DCI switch combination that drives the flux vector by directly applying the appropriate voltages to the DSSM windings [2],[13].

The stator voltage estimator is computed using:

$$\begin{pmatrix} \hat{v}_\alpha \\ \hat{v}_\beta \end{pmatrix} = A \cdot \begin{pmatrix} \hat{v}_{s1} \\ \hat{v}_{s2} \end{pmatrix} \quad (9)$$

With:

$$\hat{v}_{s1} = [\hat{v}_{a1} \ \hat{v}_{b1} \ \hat{v}_{c1}] \text{ and } \hat{v}_{s2} = [\hat{v}_{a2} \ \hat{v}_{b2} \ \hat{v}_{c2}]$$

The components of stator flux can be estimated:

$$\begin{cases} \hat{\phi}_\alpha(t) = \int_0^t (\hat{v}_\alpha - R_s \cdot i_\alpha) d\tau + \hat{\phi}_\alpha(0) \\ \hat{\phi}_\beta(t) = \int_0^t (\hat{v}_\beta - R_s \cdot i_\beta) d\tau + \hat{\phi}_\beta(0) \end{cases} \quad (10)$$

The stator flux magnitude is given by:

$$|\hat{\phi}_s| = \sqrt{\hat{\phi}_\alpha^2 + \hat{\phi}_\beta^2} \quad (11)$$

The stator flux angle is estimated by:

$$\hat{\theta}_s = \tan^{-1} \left(\frac{\hat{\phi}_\beta}{\hat{\phi}_\alpha} \right) \quad (12)$$

The torque can be expressed by:

$$T_{em} = p(\hat{\phi}_\alpha \cdot i_\beta - \hat{\phi}_\beta \cdot i_\alpha) \quad (13)$$

Tables 2 and 3 give the switching selection table of the conventional DTC for DSSM.

Table 2: DTC switching table applied on the first inverter

\emptyset	τ	Zi	\emptyset	τ	Zi	\emptyset	τ	Zi
	4	$v(i+4)L1$	4	$v(i+6)L1$	4	$v(i+8)L1$		
	3	$v(i+4)L2$	3	$v(i+6)L2$	3	$v(i+8)L2$		
	2	$v(i+4)M$	2	$v(i+6)M$	2	$v(i+8)M$		
	1	$v(i+4)S$	1	$v(i+6)S$	1	$v(i+8)S$		
1	0	$v0$	0	$v0$	-1	$v0$		
	-1	$v(i+20)S$	-1	$v(i+18)S$	-1	$v(i+16)S$		
	-2	$v(i+20)M$	-2	$v(i+18)M$	-2	$v(i+16)M$		
	-3	$v(i+20)L2$	-3	$v(i+18)L2$	-3	$v(i+16)L2$		
	-4	$v(i+20)L1$	-4	$v(i+18)L1$	-4	$v(i+16)L1$		

Table 3: DTC switching table applied on the second inverter

\emptyset	τ	Zi	\emptyset	τ	Zi	\emptyset	τ	Zi
	4	$v(i+2)L1$	4	$v(i+4)L1$	4	$v(i+6)L1$		
	3	$v(i+2)L2$	3	$v(i+4)L2$	3	$v(i+6)L2$		
	2	$v(i+2)M$	2	$v(i+4)M$	2	$v(i+6)M$		
	1	$v(i+2)S$	1	$v(i+4)S$	1	$v(i+6)S$		
1	0	$v0$	0	$v0$	-1	$v0$		
	-1	$v(i+18)S$	-1	$v(i+16)S$	-1	$v(i+14)S$		
	-2	$v(i+18)M$	-2	$v(i+16)M$	-2	$v(i+14)M$		
	-3	$v(i+18)L2$	-3	$v(i+16)L2$	-3	$v(i+14)L2$		
	-4	$v(i+18)L1$	-4	$v(i+16)L1$	-4	$v(i+14)L1$		

5 Extended Kalman Filter

The Kalman filter is a state observer that establishes the best approximation by minimization of the square error for the state variables of a system, subjected at both its input and output to random disturbances. If the dynamic system of which the state is being observed is nonlinear, then the Kalman filter is called an extended one [8], [12]. The development of the Kalman filter is closely linked to the stochastic systems. The system is described by the following equation:

$$\begin{cases} \dot{x}(t) = A.x(t) + B.u(t) + w(t) \\ y(t) = C.x(t) + v(t) \end{cases} \quad (14)$$

Where: w and v are the system and measurement noise.

The model of DSSM in the reference can be written in the following form:

$$\begin{cases} \dot{x}(t) = A.x(t) + B.u(t) \\ y(t) = C.x(t) + v(t) \end{cases} \quad (15)$$

With:

$$x(t) = [i_\alpha \ i_\beta \ \phi_\alpha \ \phi_\beta \ \Omega \ \theta]$$

$$y = [i_\alpha \ i_\beta]$$

$$u = [v_\alpha \ v_\beta]$$

$$A = \begin{bmatrix} -R_s & -p.\Omega.L_q & 0 & p.\Omega & 0 & 0 \\ p.\Omega.L_q & -R_s & -p.\Omega & 0 & 0 & 0 \\ -R_s & 0 & 0 & 0 & 0 & 0 \\ 0 & -R_s & 0 & 0 & 0 & 0 \\ -p.\phi_{beta}/J & p.\phi_{alpha}/J & 0 & 0 & -f/J & 0 \\ 0 & 0 & 0 & 0 & p & 0 \end{bmatrix}$$

$$B = \begin{bmatrix} \frac{1}{L_q} & 0 & 0 \\ 0 & \frac{1}{L_q} & 0 \\ 1 & 0 & 0 \\ 0 & 1 & 0 \\ 0 & 0 & \frac{-f}{J} \\ 0 & 0 & 0 \end{bmatrix}$$

With:

$$\begin{cases} \phi_\alpha = L_q.i_\alpha + \phi_f.\cos(\theta) \\ \phi_\beta = L_q.i_\beta + \phi_f.\sin(\theta) \end{cases}$$

The corresponding discrete time model is given:

$$\begin{cases} x_{(k+1)} = A_d.x_{(k)} + B_d.u_{(k)} \\ y_{(k+1)} = C_d.x_{(k)} \end{cases} \quad (16)$$

The conversion is done by the following approxima-

tion:

$$\begin{cases} A_d = e^{At} = I + A.T_s \\ B_d = \int_0^t .e^{A\xi} B.d\xi = B.T_s \\ C_d = C \end{cases} \quad (17)$$

6 DTC Based on Artificial Neural Networks

While there are many types of ANN, but the usual model is the multilayer feed forward network using the error back propagation algorithm [7]. This neural network has three layers: input layers, hidden layers and output layers. Each layer is composed of several neurons. The number of neurons in the input and output layers depends on the number of the selected input and output variables. The number of hidden layers and the number of neurons in each depend on the desired degree of accuracy [10].

Figure 3 shows a DTC-ANN structure consisting of a neural network with 3 linear input nodes, 12 neurons in the hidden layer, and 3 neurons in the output layer.

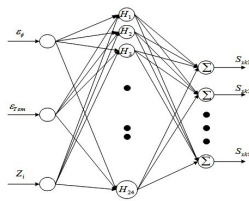


Figure 3: Neural network structure for DTC

The general structure of the DSSM with five-level sensorless DTC-ANN is represented by figure 4.

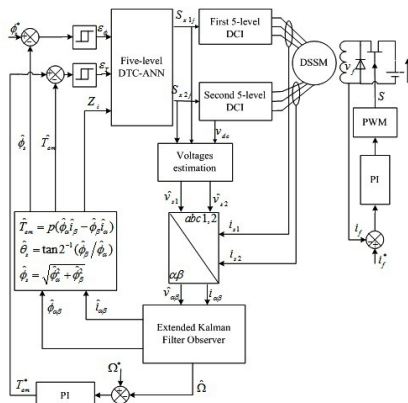
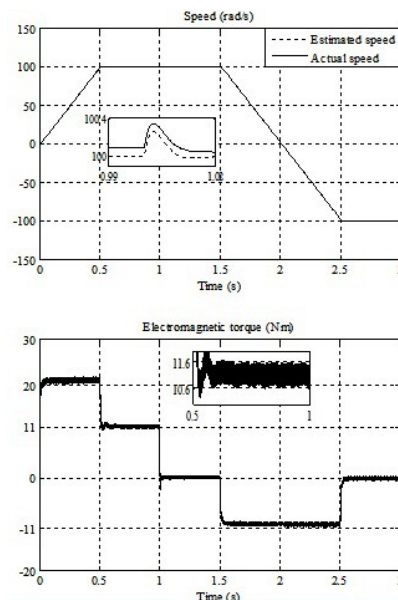


Figure 4: Neural network DTC for sensorless DSSM

7 Simulation Results of Five-Level DTC-ANN

The simulation results are obtained using the following DC link capacitor values $C_1 = C_2 = C_3 = C_4 = 1mF$. The DC side of the inverter is supplied by a constant DC source $v_{dc} = 600V$. The system was simulated using the DSSM parameters given in the Appendix.

The DSSM accelerates from standstill to reference speed $100rad/s$ with full load torque ($T_L = 11 N.m$). Afterwards, a step variation on the load torque ($T_L = 0 N.m$) is applied at time $t = 1 s$. And then a sudden reversion in the speed command from $100 rad/s$ to $-100 rad/s$ at time $1.5 s$ is performed. The obtained five-level sensorless DTC-ANN results are shown in figure 5.



It can be seen in figure 5 that the estimated and actual speeds follow their reference value. The electromagnetic torque returns to its reference value with a slight error. The torque and flux responses show excellent dynamic performances.

The instability of the four DC voltages of the intermediate capacitors filter can be seen. Indeed, the voltages v_{c2} and v_{c3} decrease whereas the voltages v_{c1} and v_{c4} increase. This result shows the problem of the unbalance of capacitor voltages and its effect on electromagnetic torque harmonics. In order to improve the performance of the five-level DTC-ANN of the sensorless DSSM, the five-level DTC-ANN based on balancing strategy is proposed in the following section.

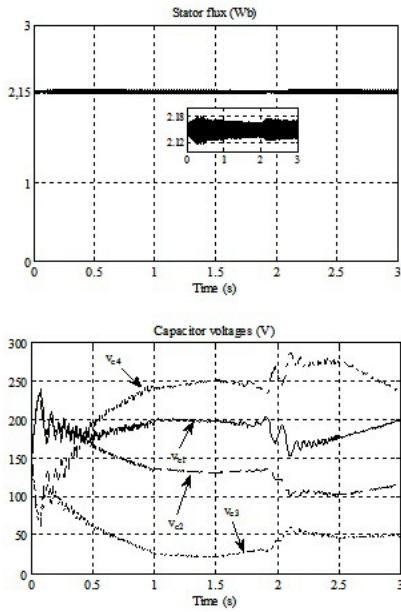


Figure 5: Dynamic responses for five-level DTC-ANN without balancing strategy of sensorless DSSM caption

8 DC-Capacitor Voltage Balancing Strategy

The DC-capacitor voltage balancing strategy is based on the minimum energy property. The idea is to minimize cost function J_k in relation to the DC-side energy using the redundant switching states of the five-level DCI units over a switching period [4]. The total energy of the four condensers is given by: $J_k = \frac{1}{2} \cdot C \sum_{j=1}^4 \Delta v_{cj}^2$

$$J_k = \frac{1}{2} \cdot C \sum_{j=1}^4 \Delta v_{cj}^2 \quad (18)$$

Where $\Delta_{cj} = v_{cj} - (v_{dc}/4)$ is a voltage deviation of capacitor, and v_{dc} is the DC-link voltage. Based on proper selection of redundant switching states of both DCI, J_k can be minimized if the capacitor voltages are maintained at their voltage reference values of $(v_{dc}/4)$ [6]. The mathematical condition to minimize J_k is:

$$\frac{dJ_k}{dt} = C \cdot \sum_{j=1}^4 \Delta v_{cj} \cdot \frac{dv_{cj}}{dt} = \sum_{j=1}^4 \Delta v_{cj} \cdot i_{cj} \leq 0 \quad (19)$$

Where i_{cj} is the current through capacitor C_j .

The capacitor currents in (19) are affected by the DC-side intermediate branch currents i_{k3} , i_{k2} , and i_{k1} . These currents can be calculated if the switching states used in the switching pattern are known. Thus, it is advantageous to express (19) in terms of i_{k3} , i_{k2} , and i_{k1} . The DC-capacitor currents are expressed as:

$$\begin{cases} i_{c4} = i_{c3} + \sum_{k=1}^2 i_{k3} \\ i_{c3} = i_{c2} + \sum_{k=1}^2 i_{k2} \\ i_{c2} = i_{c1} + \sum_{k=1}^2 i_{k1} \end{cases} \quad (20)$$

The DC-capacitor currents are expressed as:

$$i_{cj} = \frac{1}{4} \sum_{y=1}^3 y \left(\sum_{k=1}^2 i_{ky} \right) - \sum_{y=j}^3 \left(\sum_{k=1}^2 i_{ky} \right) \quad (21)$$

Substituting i_{cj} from (21) into (19), the following condition to achieve voltage balancing is deduced:

$$\sum_{j=1}^4 \Delta v_{cj} \left(\frac{1}{4} \sum_{y=1}^3 y \left(\sum_{k=1}^2 i_{ky} \right) - \sum_{y=j}^3 \left(\sum_{k=1}^2 i_{ky} \right) \right) \leq 0 \quad (22)$$

Imposing:

$$\sum_{j=1}^4 \Delta v_{cj} = 0 \quad (23)$$

Substituting Δv_{c4} calculated from (23) into (25)

$$\sum_{j=1}^3 \Delta v_{cj} \left(\sum_{y=j}^3 \left(\sum_{k=1}^2 i_{ky} \right) \right) \geq 0 \quad (24)$$

Applying the averaging operator, over one sampling period, to (24) results in:

$$\frac{1}{T} \sum_{KT}^{(K+1)T} \Delta v_{cj} \left(\sum_{y=j}^3 \left(\sum_{k=1}^2 i_{ky} \right) \right) dt \geq 0 \quad (25)$$

Assuming that both DCI units have the same sampling period T , and since T is fairly short compared to the time interval associated with the dynamics of each capacitor voltage, capacitor voltages can be assumed

as constant values over T and consequently, (25) is simplified to:

$$\sum_{j=1}^3 \Delta v_{cj}(k) \left(\sum_{y=j}^3 \frac{1}{T} \int_{KT}^{(K+1)T} \left(\sum_{k=1}^2 \bar{i}_{ky} \right) \right) dt \geq 0 \quad (26)$$

Or

$$\sum_{j=1}^3 \Delta v_{cj}(k) \left(\sum_{y=j}^3 \left(\sum_{k=1}^2 \bar{i}_{ky}(k) \right) \right) dt \geq 0 \quad (27)$$

So, the cost function at sampling period K is given by:

$$J_k = \sum_{j=1}^3 \Delta v_{cj}(k) \left(\sum_{y=j}^3 \left(\sum_{k=1}^2 \bar{i}_{ky}(k) \right) \right) \quad (28)$$

Where: $\Delta v_{cj}(k)$ is the voltage drift of C_j at sampling period K , and $\bar{i}_{ky}(k)$ is the averaged value of the y^{th} DC-side intermediate branch current. Currents $i_{ky}(k)$ should be computed for different combinations of adjacent redundant switching states over a sampling period and the best combination which maximizes (28) is selected.

When the tip of the reference voltage vector is located in zone (Z_i), the average values of DC-side intermediate branch currents are:

$$\bar{i}_{ky} = i_{ky} \quad (29)$$

To calculate $y = 1, 2, 3$, the contributions of switching states to the DC-side intermediate branch currents, and the relationship between the DC and AC side currents i_{ak} , i_{bk} , and i_{ck} are required. Thus, the currents of the inverter input are expressed according to the currents i_{k1} , i_{k2} and i_{k3} by means of the functions of connection of the half-arms by the following relations:

$$i_{ky} = F_{caky} \cdot i_{ak} + F_{cbky} \cdot i_{bk} + F_{ccky} \cdot i_{ck} \quad (30)$$

The relationship between the switching states can also be exploited to deduce the relationships between i_{k1} , i_{k2} , i_{k3} and i_{ak} , i_{bk} , i_{ck} . For each set of switching combinations, the currents i_{ky} are

calculated based on (29) and replaced in (28). The best set that fulfills the condition is selected.

A schematic block representation of the five-level DTC-ANN including the DC capacitor voltage control block is depicted in figure 6.

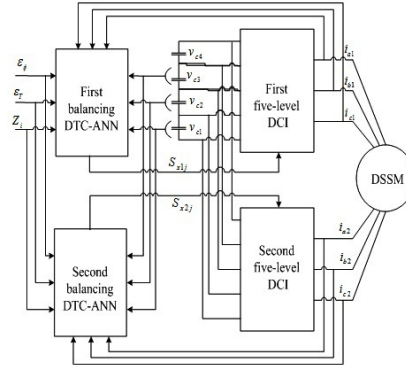


Figure 6: Schematic representation of the five-level DTC-ANN with balancing strategy

9 Simulation Results of Five-Level DTC-ANN with Balancing Strategy

Figure 7 sets out the simulation results obtained in the same conditions as in figure 5.

Note that the actual and estimated speed responses are merged with the reference one and the stator flux follows its reference value. The decoupling control between electromagnetic torque and stator flux is always confirmed. Moreover, the stator flux and electromagnetic torque ripples are clearly reduced.

It can be observed that the proposed balancing strategy is able to guarantee capacitor voltage balance even during the abovementioned transits.

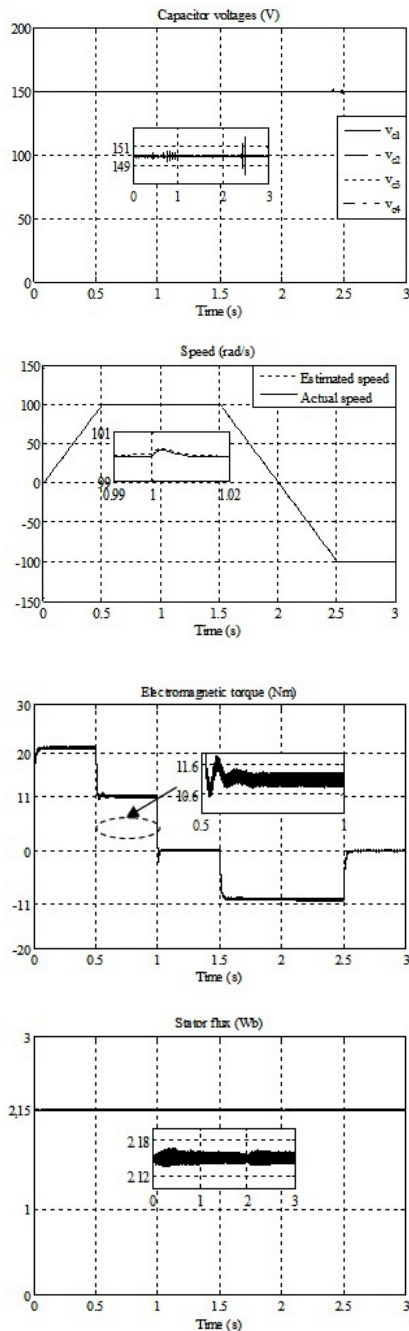


Figure 7: Dynamic responses for five-level DTC-ANN with balancing strategy of sensorless DSSM

10 Conclusion

This paper presents a DTC-ANN applied sensorless DSSM using extended Kalman filter. The output switching states vectors of the ANN controller are used to control the two five-level DCI. This multilevel DCI topology has the inherent problem of DC-link capacitor voltage variations. For this reason, the DTC-ANN with balancing strategy based on minimization

of energy property is proposed to balance the voltage across each of the DC-link capacitors. The simulation results demonstrate that the proposed DTC-ANN can maintain the decoupling between the flux and torque and carry out voltage balancing. Moreover, the robustness of the observer against speed and load variations confirms the good dynamic performance of the developed sensorless multiphase drive. Furthermore, by means of the five-level DTC drive, it is possible to reduce the stress of the switching devices of the DCI and lower switching power losses, which are frequent requirements of high power applications.

11 Declaration of conflicting interest

This work was supported by the Directorate-General for Scientific Research and Technological Development (DG-RSDT) of Algeria under PRFU project number A01L07UN300120200001.

12 Appendix

DSSM machine parameters are listed in table 4.

Table 4: DSSM Parameters

Components	Sym- bol	Rating values
Stator resistance	R_s	2.35Ω
Rotor resistance	R_f	30.3Ω
d-axis stator inductance	L_d	$0.3811H$
q-axis stator inductance	L_q	$0.211H$
Rotor inductance	L_f	$15 H$
Mutual inductance	M_{fd}	$2.146 H$
Moment of inertia	J	$0.05Nms^2/rad$
Friction coefficient	f	$0.001Nms/rad$
Active power	P	$5 kW$
Number of pole	p	2
Voltage	V	$232 V$
Frequency	f	$50 Hz$

References

- [1] W.-R. Canders and H. Mosebach. Multiphase machines with individual slot activation. *Electrical Engineering*, 100(4):2287–2297, jun 2018.
- [2] L. Schreier, J. Bendl, and M. Chomat. Analysis of influence of third spatial harmonic on currents and torque of multi-phase synchronous machine with permanent magnets. *Electrical Engineering*, 100(3):2095–2102, mar 2018.
- [3] Rutuja Pawar, S.P. Gawande, S.G. Kadwane, M.A. Waghmare, and R.N. Nagpure. Five-Level Diode Clamped Multilevel Inverter (DCMLI) Based Electric Spring for Smart Grid Applications. *Energy Procedia*, 117:862–869, jun 2017.
- [4] Huaitian Zhang, Harith R. Wickramasinghe, Long Jing, Jinke Li, Josep Pou, and Georgios Konstantinou. Circulating current control scheme of modular multilevel converters supplying passive networks under unbalanced load conditions. *Electric Power Systems Research*, 171:36–46, jun 2019.
- [5] Dongdong Cui and Qiongquan Ge. A Novel Hybrid Voltage Balance Method for Five-Level Diode-Clamped Converters. *IEEE Transactions on Industrial Electronics*, 65(8):6020–6031, aug 2018.
- [6] Shunji Shi, Xiangzhou Wang, Shuhua Zheng, Yanxi Zhang, and Dongyuan Lu. A New Diode-Clamped Multilevel Inverter With Balance Voltages of DC Capacitors. *IEEE Transactions on Energy Conversion*, 33(4):2220–2228, dec 2018.
- [7] Han Jiang, Zhongli Xi, Anas A. Rahman, and Xiaoqing Zhang. Prediction of output power with artificial neural network using extended datasets for Stirling engines. *Applied Energy*, 271:115123, aug 2020.
- [8] Tarek Ameid, Arezki Menacer, Hicham Talhaoui, and Imadeddine Harzelli. Rotor resistance estimation using Extended Kalman filter and spectral analysis for rotor bar fault diagnosis of sensorless vector control induction motor. *Measurement*, 111:243–259, dec 2017.
- [9] A. Naserbegi, M. Aghaie, and S.M. Mahmoudi. PWR core pattern optimization using grey wolf algorithm based on artificial neural network. *Progress in Nuclear Energy*, 129:103505, nov 2020.
- [10] A. Ghamri, R. Boumaaraf, M.T. Benchouia, H. Mesloub, A. Goléa, and N. Goléa. Comparative study of ANN DTC and conventional DTC controlled PMSM motor. *Mathematics and Computers in Simulation*, 167:219–230, jan 2020.
- [11] Hang Seng Che, Ayman Samy Abdel-Khalik, Obrad Dordevic, and Emil Levi. Parameter Estimation of Asymmetrical Six-Phase Induction Machines Using Modified Standard Tests. *IEEE Transactions on Industrial Electronics*, 64(8):6075–6085, aug 2017.
- [12] Mehmet Ali Usta, Halil Ibrahim Okumus, and Hakan Kahveci. A simplified three-level SVM-DTC induction motor drive with speed and stator resistance estimation based on extended Kalman filter. *Electrical Engineering*, 99(2):707–720, oct 2016.
- [13] Radhwane SADOUNI. Three Level DTC-SVM for Dual Star Induction Motor Fed by Two Cascade VSI with DPCVF-SVM Rectifier. *Journal of Power Technologies*, 100(2), 2020.